

Motor Imagery Decoding Using Ensemble Curriculum Learning and Collaborative Training

Georgios Zoumpourlis and Ioannis Patras *Senior Member, IEEE*

Abstract—Objective: In this work, we study the problem of cross-subject motor imagery (MI) decoding from electroencephalography (EEG) data. Multi-subject EEG datasets present several kinds of domain shifts due to various inter-individual differences (e.g. brain anatomy, personality and cognitive profile). These domain shifts render multi-subject training a challenging task and also impede robust cross-subject generalization. **Method:** We propose a two-stage model ensemble architecture, built with multiple feature extractors (first stage) and a shared classifier (second stage), which we train end-to-end with two loss terms. The first loss applies curriculum learning, forcing each feature extractor to specialize to a subset of the training subjects and promoting feature diversity. The second loss is an intra-ensemble distillation objective that allows collaborative exchange of knowledge between the models of the ensemble. **Results:** We compare our method against several state-of-the-art techniques, conducting subject-independent experiments on two large MI datasets, namely Physionet and OpenBMI. Our algorithm outperforms all of the methods in both 5-fold cross-validation and leave-one-subject-out evaluation settings, using a substantially lower number of trainable parameters. **Conclusion:** We demonstrate that our model ensembling approach combining the powers of curriculum learning and collaborative training, leads to high learning capacity and robust performance. **Significance:** Our work addresses the issue of domain shifts in multi-subject EEG datasets, paving the way for calibration-free BCI systems.

Index Terms—Brain-Computer Interface (BCI), electroencephalography (EEG), motor imagery, domain generalization

I. INTRODUCTION

BRAIN-COMPUTER INTERFACES (BCIs) [51] are communication systems that enable human users to interact with computers, robotic limbs or wheelchairs, translating brain activity into commands. BCIs have a wide spectrum of applications, including post-stroke rehabilitation of limb motor impairments [6], character typing through visual spellers [50] and interactive image generation [45]. The operation of BCI systems leverages neuroimaging techniques to collect brain signals, with the most prevalent one being electroencephalography (EEG) [1], [8]. Advancing EEG-based BCIs towards out-of-the-lab settings, requires equipping them with machine learning models that have robust cross-subject generalization.

With the advent of deep learning (DL), significant steps have been made in the exploration of training methodologies and model architectures [20] that can accommodate learning from EEG datasets with increasingly large number of participants.

The work of Georgios Zoumpourlis was supported by QMUL Principal’s Studentship.

Georgios Zoumpourlis and Ioannis Patras are with the School of Electronic Engineering and Computer Science, Queen Mary University of London, London E1 4NS, United Kingdom. E-mail: {g.zoumpourlis, i.patras}@qmul.ac.uk.

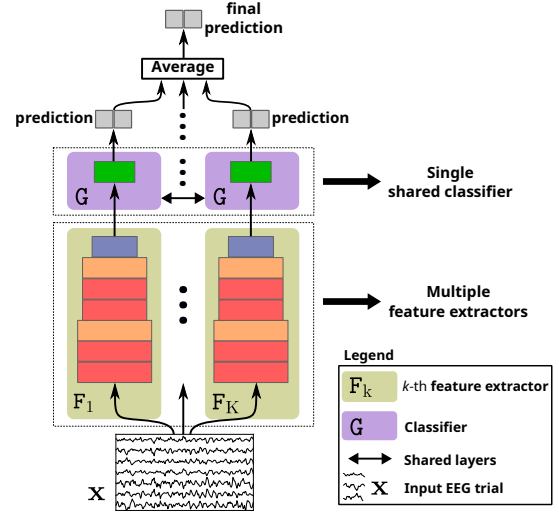


Fig. 1: Overview of our proposed ensemble architecture during inference. First, an input EEG trial is fed to multiple feature extractors that produce diverse feature representations. Then, a single shared classifier predicts the class scores corresponding to each feature representation, and these class scores are averaged to compute the final prediction.

Inter-subject variability is one of the biggest challenges in the field of EEG-based BCIs, referring to the existence of differences in the characteristics of EEG signals acquired from different individuals (i.e., there are different data distributions for each subject) [35]. In the literature, often the data of each individual are considered as a separate domain [28], hence the inter-subject differences are treated as domain shifts.

In this work, we consider the problem of EEG-based motor imagery (MI) decoding in subject-independent settings. Motor imagery is a well-known paradigm for BCIs, involving the imagination of motor acts, without overt motor execution or muscle activation [34]. The usage of the MI paradigm is based on the phenomenon of sensorimotor rhythms [52], i.e. rhythmic oscillations over the sensorimotor cortex, that arise during motor imagery. There are several sources of variation that lead to domain shifts in cross-subject MI decoding problems, such as personality type, cognitive profile, neurophysiological predictors, brain anatomy and familiarity with BCI technology [24], [25]. These variations in turn lead to spatial, spectral and temporal differences in the manifestation of sensorimotor rhythms across individuals [40]. These differences are the sources of domain shifts that we aim to overcome in order to obtain robust performance in subject-independent settings.

Under this perspective, two learning paradigms have been widely explored to build convolutional neural networks (CNNs) with strong subject-independent performance: domain adaptation and domain generalization. In domain adaptation, the goal is to reduce the domain shift using either solely labelled [21] or unlabelled [33] data from the target domain. Evidently, the requirement to have available data from the target domain (i.e. a test subject) during the training phase is a limiting factor. By contrast, the goal of domain generalization is generalizing to new (unseen) target domains without requiring any data from them, which is more attractive for subject-independent EEG-based BCI systems.

A category of domain generalization techniques [47] that has been successfully applied on EEG-based problems [5], [39] is ensemble learning [55]. A resulting property of ensembling is the emergence of diverse feature representations, leading to better generalization. However, existing ensembling works achieve this diversity at the cost of increased computational complexity, lengthy model selection processes and less generic feature extractors. In the complex ensemble architecture of InceptionEEG-Net (IENet) [15], each individual CNN model has more than seventy convolutional layers. The model ensemble proposed by Dolzhikova *et al.* [14] requires multiple hyperparameter tuning runs to train each base model. In the method of Chadaklar *et al.* [12], a deep ensemble model builds on handcrafted features, extracted from the subject-specific algorithm of Filter Bank CSP [3].

Hence, some disadvantages of existing ensemble learning works are that they rely on complex architectures, do not support end-to-end training in a single phase and build on subject-specific models. Differently from works that require multiple training runs [5], [14], [39], our method involves training a single model in an end-to-end manner. Moreover, in contrast to Chadaklar *et al.* [12], we refrain from combining individual models that are trained on a single subject each, as this compromises their generalization capabilities. Compared to IENet [15], our ensemble is composed from base models that have a compact and simplistic architecture.

We frame our approach as a model ensembling method combined with: (i) a curriculum learning strategy to promote the diversity across individual models and (ii) a collaborative training scheme to exchange knowledge between the models through a distillation loss. We design a training curriculum, such that each model of the ensemble is trained on *all* the source domains (i.e. training subjects), but progressively specializes to a specific subset of subjects. This leads each model to capture patterns that are mostly specific to the EEG signal characteristics of a subset of training subjects, rather than the entire training set. Training our architecture under such a curriculum, equips it with strong generalization capabilities, by covering a wide range of patterns through several models that act as diverse feature extractors. To regulate the trade-off between diversity and generalization [9], we introduce an intra-ensemble distillation loss that pushes the predictions of each individual model close to the average of the predictions of all the other models, thereby controlling the diversity within the ensemble. This is done by using pseudolabels (obtained from the predictions of all the other models) as groundtruth

targets for each model. In essence, our collaborative training scheme leads to distillation of knowledge *across* the models, working complementary with the curriculum that is designed for *each* model. The balance between diversity and generalization is controlled through a hyperparameter that weighs the contribution of the pseudolabel-based loss to the total loss.

Our contributions are the following:

- We propose a model ensembling architecture which we pair with a novel curriculum learning scheme. Our curriculum promotes diversity across the models of the ensemble, driving each model to specialize to a different subset of training subjects. To our knowledge, curriculum learning has not been previously explored for cross-subject MI decoding.
- We propose an auxiliary intra-ensemble distillation loss, allowing the exchange of knowledge between the individual models of the ensemble. This balances the diversity-generalization trade-off, leading to further performance improvement. Our work is the first to propose a pseudolabelling scheme for EEG-based knowledge distillation.
- We conduct our experimental analysis on two large motor imagery datasets (Physionet [16] and OpenBMI [32]) totalling more than 150 subjects. We compare our method against four state-of-the-art techniques, namely TID-Net [28], EEGSym [38], MIN2Net [4] and ATL [54], showing superior results.
- We make our code publicly available¹ to support reproducibility.

The rest of the manuscript is organized as follows. In Section II we outline relevant previous works, while in Section III we describe our proposed method. In Section IV we present the results of our experimental analyses and ablation studies. Lastly, in Section V we conclude the manuscript.

II. RELATED WORK

In this Section, we present an overview of the related work on the topics of domain generalization, ensemble learning and feature diversity.

Domain generalization: A much larger volume of works has been published on visual data, compared to the works on EEG data. Regarding learning from visual data, there is a line of works that claim various benefits, however upon a rigorous comparison, Gulrajani *et al.* [17] show that the trivial approach of Empirical Risk Minimization (ERM) [46] can, if carefully tuned, outperform several state-of-the-art domain generalization techniques. Several works building subject-independent models for EEG data (which by nature is a domain generalization problem), do not explicitly take care of inter-subject variability [4], [38], [56]. Such methods adopt ERM-based approaches that simply minimize the training loss over all source domains (i.e. training subjects). Apart from the effective ERM baseline, other methods that have been occasionally used for multi-subject EEG training are MixUp [28], [53] (which was initially proposed for visual data) and Euclidean/Riemannian Alignment (EA/RA) [19],

¹<https://github.com/gzoumpourlis/Ensemble-MI>

[28], [49]. Alignment methods such as EA/RA are powerful domain generalization baselines for learning domain-invariant representations, which can be combined with other multi-domain learning techniques [28]. By contrast, MixUp has been found to have a rather detrimental effect on multi-subject training [28]. In our work, we leverage the benefits of RA, along with our proposed curriculum learning and intra-ensemble distillation techniques.

Ensemble learning: Model ensembling [18] is ubiquitous in the applications of machine learning on EEG data [44]. Combining the predictions of multiple models has been tried both in intra-subject [37] and subject-independent [41] settings, using variants of the Common Spatial Pattern (CSP) [10], [27] algorithm. The fact that CSP methods extract handcrafted features is a restricting factor, and their cross-subject generalization capabilities have been shown to be poor. A successful example of model ensembling using CNNs is the work of Bakas *et al.* [5], where a k -fold cross validation process results in k trained models, with each model trained on data from all the available training subjects. Reuben *et al.* [39] leverage the power of available crowdsourced algorithms for an EEG-based seizure prediction competition [29], exploring the possibility of obtaining performance improvements by combining them through model ensembling.

Feature diversity: One of the key properties of ensemble learning, is the emergence of diverse feature representations across the individual base models of ensembles. However, feature diversity can also be obtained through alternative techniques which do not fall within the category of ensemble learning, as they explore ways to obtain diverse features through a single model. Ma *et al.* [36] propose a multi-branch network architecture where the input EEG signal is divided in four frequency bands, with a dedicated branch for each band. Altuwaijri *et al.* [2] introduce a multi-branch network based on EEGNet [31], where each branch contains a different number of temporal filters, as well as a different temporal filter length. A network capable of processing spectral-spatial representations as inputs is presented by Kwon *et al.* [30].

We draw inspiration from Wei *et al.* [48], where a multi-branch Separate-Common-Separate Network (SCSN) is proposed to tackle the issue of negative transfer learning. Negative learning can appear when training subject-agnostic feature extractors, i.e. when all the layers of a single model are trained on all the training subjects. As a remedy to this, SCSN has a separate feature extractor for each training subject. However we claim that such an approach leads to non-optimal solutions, as training subject-specific layers compromises their generalization capability. We propose a model ensembling approach that differs from these two scenarios (i.e. subject-specific or subject-agnostic layers), yet combines the best of both worlds. In contrast to SCSN [48], we train multiple feature extraction models on all training subjects, yet we guide each individual feature extractor to specialize on a subset of multiple subjects.

III. PROPOSED METHOD

In this section we describe the proposed methodology, which consists of a model ensemble architecture, a curriculum

training scheme and an intra-ensemble distillation loss. We provide an overview of the training pipeline for our proposed architecture in Fig. 2 and present its individual components in the following subsections. Specifically, we begin by explaining our ensemble architecture in Subsection III-A. Then, we introduce the first loss term that materializes our curriculum learning scheme in Subsection III-B, as well as the second loss term that enables collaborative training across the models of the ensemble, in Subsection III-C.

A. Architecture

1) *Single model:* In this work, we use the well-established EEGNet [31] architecture as our strong single-model baseline. The selection of EEGNet is justified from the fact that it achieves compelling performance, with a reasonably small number of trainable parameters and a simple network design (e.g. without streams of varying kernel lengths, or band-wise processing streams). In the task of MI decoding, the time-series signals $\mathbf{x} \in \mathbb{R}^{C \times T}$ of an EEG trial with C electrodes and T samples in the temporal dimension, are fed as input to EEGNet. The class-wise scores $\hat{\mathbf{y}} \in \mathbb{R}^{N_C}$ (where N_C is the number of classes) are obtained as output, while the groundtruth label $\mathbf{y} \in \mathbb{R}^{N_C}$ is represented in the form of a one-hot vector. Thus, in the case of EEGNet the output scores are computed as

$$\hat{\mathbf{y}} = \text{EEGNet}(\mathbf{x}), \quad (1)$$

and the network is optimized by minimizing the cross-entropy (CE) loss $\mathcal{L}_{\text{CE}} = \text{CE}(\hat{\mathbf{y}}, \mathbf{y})$, given by

$$\text{CE}(\hat{\mathbf{y}}, \mathbf{y}) = - \sum_{i=1}^{N_C} y_i \log(\text{softmax}(\hat{y}_i)), \quad (2)$$

where y_i and \hat{y}_i are the i -th elements of \mathbf{y} and $\hat{\mathbf{y}}$ respectively.

2) *Model ensemble:* Our model ensemble architecture (shown in Fig. 2) consists of two stages and uses EEGNet as its elementary component. The first stage contains multiple models in parallel, with all models having exactly the same architecture design. These models act as feature extractors on an input sample, with each model producing a feature vector. We use $F_k(\cdot)$ and \mathbf{f}_k to denote the k -th feature extractor and its output feature vector. The output feature vectors from the first stage, are computed as

$$[\mathbf{f}_1, \mathbf{f}_2, \dots, \mathbf{f}_K] = [F_1(\mathbf{x}), F_2(\mathbf{x}), \dots, F_K(\mathbf{x})]. \quad (3)$$

The second stage has a single shared classification head $G(\cdot)$, that computes the class-wise prediction scores for each feature vector originating from the first stage. We use $\hat{\mathbf{y}}_k$ to denote the scores corresponding to the k -th feature vector \mathbf{f}_k . The scores are computed as

$$[\hat{\mathbf{y}}_1, \hat{\mathbf{y}}_2, \dots, \hat{\mathbf{y}}_K] = [G(\mathbf{f}_1), G(\mathbf{f}_2), \dots, G(\mathbf{f}_K)]. \quad (4)$$

In the simple scenario where no curriculum learning occurs, this architecture is trained by minimizing the sum of the individual losses for the predictions of each model. The loss $\mathcal{L}_{\text{CE}}^k$ for the predictions $\hat{\mathbf{y}}_k$ of the k -th model, and the total loss $\mathcal{L}_{\text{CE}}^{\text{total}}$, are computed as

$$\mathcal{L}_{\text{CE}}^k = \text{CE}(\hat{\mathbf{y}}_k, \mathbf{y}) \quad (5)$$

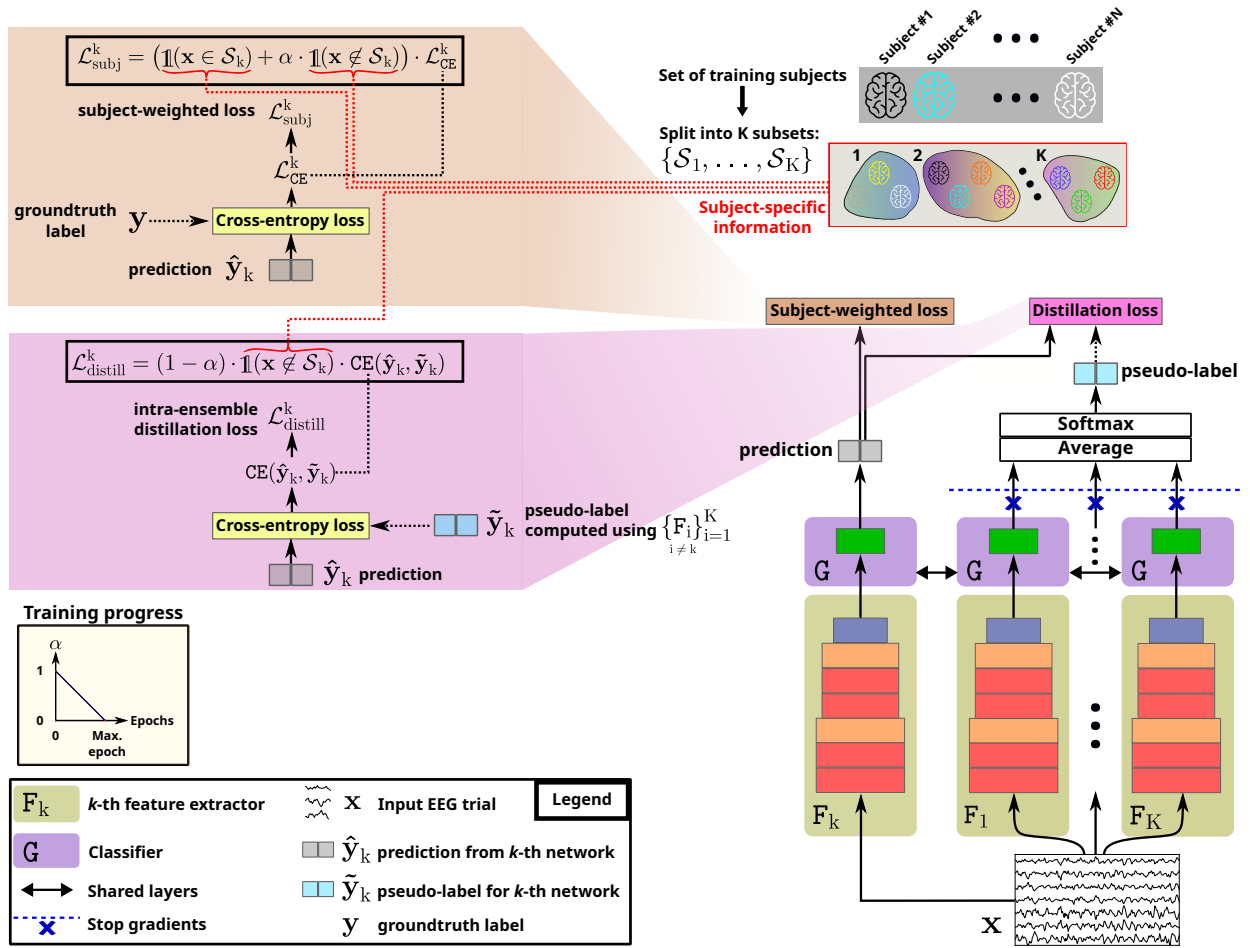


Fig. 2: Our proposed architecture has K first stage models and a shared classifier in the second stage. The input trial x is separately passed to each one of the first stage models, obtaining the feature vectors $[f_1, f_2, \dots, f_K]$ (Eq. 3). For the k -th model, the class-wise scores \hat{y}_k are computed by forwarding f_k to the shared classifier of the second stage (Eq. 4). In an ensembling scenario where the architecture is trained without curriculum learning, we compute the individual model losses \mathcal{L}_{CE}^k (Eq. 5) and minimize the loss $\mathcal{L}_{CE}^{\text{total}}$ (Eq. 6) for all models. In the ensemble curriculum learning scenario, we compute the individual subject-weighted losses $\mathcal{L}_{\text{subj}}^k$ (Eq. 9) and minimize the loss $\mathcal{L}_{\text{subj}}^{\text{total}}$ (Eq. 10) for all models. When also performing collaborative training, we additionally compute the losses $\mathcal{L}_{\text{distill}}^k$ (Eq. 12) and minimize the total loss $\mathcal{L}_{\text{total}}$ (Eq. 14) for all models.

$$\mathcal{L}_{CE}^{\text{total}} = \sum_{k=1}^K \mathcal{L}_{CE}^k. \quad (6)$$

In the inference phase, to classify an input sample x we fuse the model-wise scores through a simple average operation and obtain a final score vector \hat{y}_{ens} as follows:

$$\hat{y}_{\text{ens}} = \frac{1}{K} \sum_{k=1}^K \hat{y}_k. \quad (7)$$

To this end, the described architecture is purely subject-agnostic, having no subject-specific layers (both in the first and second stage). In the following subsection we propose an ensemble curriculum learning scheme that is applied during training and changes the nature of the first stage layers. Our curriculum provides a strong alternative to the typical subject-agnostic layers, that can be adopted in ensemble learning.

B. Ensemble curriculum learning

Our goal is to make each feature extractor to specialize on a specific subset of subjects. That is, we want to induce *local* (i.e. focused on a subset of the entire training set) feature extraction power to each model in the first stage. Let $\mathcal{D} = \{\mathcal{D}_1, \mathcal{D}_2, \dots, \mathcal{D}_N\}$ be a dataset with the data of N subjects, where \mathcal{D}_n denotes the sub-dataset containing the trials of the n -th subject. For an ensemble with K models ($K \geq 2$), we split \mathcal{D} into K non-overlapping subsets \mathcal{S} : $\mathcal{D} = \{\mathcal{S}_1, \dots, \mathcal{S}_K\}$. We do this splitting process by randomly assigning the sub-dataset of each subject to one of the K subsets, with a uniform probability for all subsets. Therefore, we have $\bigcup_{k=1}^K \mathcal{S}_k = \mathcal{D}$ and $\mathcal{S}_i \cap \mathcal{S}_j = \emptyset$ for $i \neq j$. Each subset \mathcal{S}_k corresponds to the k -th model and contains the sub-datasets of the subjects on which we drive the k -th model to specialize.

To achieve this specialization, we design a *subject-weighted* loss function where we inject subject-specific coefficients to weigh the contribution of each subject to the loss of each

model. Considering the subject-weighted loss $\mathcal{L}_{\text{subj}}^k$ that is used to train the k -th model, the subject-specific coefficients linearly decay over epochs the loss contribution of the subjects that *do not* belong to \mathcal{S}_k . Effectively, this makes the k -th model to focus more on the subjects of \mathcal{S}_k that have a non-decaying loss contribution. We scale the contribution of a training sample \mathbf{x} to the loss $\mathcal{L}_{\text{subj}}^k$ through the coefficient $\beta(\mathbf{x}, k)$. If trial \mathbf{x} corresponds to a subject that belongs in \mathcal{S}_k (hence $\mathbf{x} \in \mathcal{S}_k$), then we keep $\beta(\mathbf{x}, k) = 1$ throughout the whole training process. Otherwise ($\mathbf{x} \notin \mathcal{S}_k$), we decay $\beta(\mathbf{x}, k)$ from 1 to 0 while training progresses, that is:

$$\beta(\mathbf{x}, k) = \begin{cases} 1 & , \text{if } \mathbf{x} \in \mathcal{S}_k \\ \alpha & , \text{if } \mathbf{x} \notin \mathcal{S}_k \end{cases}, \quad (8)$$

where $\alpha = 1 - \frac{\text{epoch}}{N_{\text{epochs}}} \in [0, 1]$ represents the progression of training, as N_{epochs} is the maximum number of training epochs and epoch is the current epoch. The loss $\mathcal{L}_{\text{subj}}^k$ of the k -th model and the total subject-weighted loss $\mathcal{L}_{\text{subj}}^{\text{total}}$ are computed as follows:

$$\mathcal{L}_{\text{subj}}^k = \underbrace{\beta(\mathbf{x}, k)}_{\text{subject-specific coefficient}} \cdot \mathcal{L}_{\text{CE}}^k \quad (9)$$

$$\mathcal{L}_{\text{subj}}^{\text{total}} = \sum_{k=1}^K \mathcal{L}_{\text{subj}}^k. \quad (10)$$

An indicative illustration of our curriculum learning scheme is shown in the supplementary material.

C. Intra-ensemble distillation for collaborative training

In this subsection we propose a collaborative training scheme which helps to regulate the diversity-generalization trade-off in our model ensemble. In order to classify a sample, we extract its first stage representations, feed them to the shared classifier of the second stage and average the individual scores across models. The diversity between the first stage representations of a sample can make the classifier to compute inconsistent class scores across models. This, in turn, can negatively affect the final prediction scores, as they will be the result of fusing multiple contradicting predictions. We observe that, although feature diversity is a desirable property of our ensemble, it can also have an adverse effect on the generalization capabilities.

To overcome this phenomenon, we introduce a loss term that promotes consistency across the multiple model predictions, in order to improve the performance of the entire ensemble. We design our proposed intra-ensemble distillation loss to operate on the predicted scores of the second stage, instead of operating on the features extracted from the first stage. An overview of our distillation loss is shown in Fig. 2. Considering each prediction $\hat{\mathbf{y}}_k$ of the k -th model, our loss pushes it closer to the softmaxed average of the predictions from all the other models (which is the pseudolabel in our distillation loss). Specifically, we compute the pseudolabel $\tilde{\mathbf{y}}_k$ for the k -th model as:

$$\tilde{\mathbf{y}}_k = \text{softmax} \left(\frac{1}{K-1} \sum_{i=1, i \neq k}^K \hat{\mathbf{y}}_i \right), \quad (11)$$

and use the cross-entropy loss between the prediction $\hat{\mathbf{y}}_k$ and the pseudolabel $\tilde{\mathbf{y}}_k$. We note that we apply a stop-gradient [13] operation on the pseudolabels, as shown in Fig. 2. We do this in order to ensure that only the weights of the k -th model are updated based on this loss term, while the other models remain unaffected. For the k -th model, we opt to *not* apply this loss on the samples of \mathcal{S}_k . This is done through a binary mask that zeroes out the distillation loss of these samples. We do so, as the k -th model is sufficiently trained on the samples of \mathcal{S}_k through their groundtruth labels \mathbf{y} .

We note that it is necessary to scale the contribution of the intra-ensemble distillation loss to the total loss of the architecture, in accordance with the progress of training. In the beginning of the training process, the weights of the architecture are randomly initialized. Hence, penalizing the distance of model predictions from the derived pseudolabels is not so meaningful in the early epochs. As training proceeds, each feature extractor progressively focuses on a subset of subjects and feature diversity increases. As shown later in the experiments, our distillation loss indirectly controls this emerging feature diversity by bringing closer the class scores computed from various first stage features. We linearly increase the contribution of the distillation loss to the total loss, across training epochs, by multiplying it with the scalar $1 - \alpha$ that quantifies the training progress.

The distillation loss $\mathcal{L}_{\text{distill}}^k$ of the k -th model, and the total distillation loss $\mathcal{L}_{\text{distill}}^{\text{total}}$ are computed as follows:

$$\mathcal{L}_{\text{distill}}^k = (1 - \alpha) \cdot \underbrace{\mathbb{1}(\mathbf{x} \notin \mathcal{S}_k)}_{\text{subject-specific mask}} \cdot \text{CE}(\hat{\mathbf{y}}_k, \tilde{\mathbf{y}}_k) \quad (12)$$

$$\mathcal{L}_{\text{distill}}^{\text{total}} = \sum_{k=1}^K \mathcal{L}_{\text{distill}}^k. \quad (13)$$

We compute the total loss $\mathcal{L}_{\text{total}}$ of our architecture as:

$$\mathcal{L}_{\text{total}} = \lambda_{\text{subj}} \cdot \mathcal{L}_{\text{subj}}^{\text{total}} + \lambda_{\text{distill}} \cdot \mathcal{L}_{\text{distill}}^{\text{total}}, \quad (14)$$

where we empirically set $\lambda_{\text{subj}} = K$ and $\lambda_{\text{distill}} = 0.7$.

IV. EXPERIMENTAL RESULTS

A. Datasets

We apply our method on the problem of motor imagery decoding and work on two large datasets: Physionet [16], [42] and OpenBMI [32]. First we provide a brief description of the datasets and then we describe the common signal preprocessing pipeline that is followed for both datasets.

Physionet dataset: The dataset contains EEG recordings from 109 participants, with trials that belong to 4 classes: left-hand, right-hand and feet imagery, as well as rest. The data are recorded with 64 EEG electrodes at a sampling frequency of 160Hz. We choose to work on the two-class problem of classifying left-hand versus right-hand imaginary movements, discarding the data from the other classes. Similarly to other works [7], [28], we also discard data from 6 participants (specifically S088, S090, S092, S100, S104 and S106) that have inconsistent sampling frequencies or trial lengths. In our experiments we use the signals from all 64 electrodes.

OpenBMI dataset: The data of OpenBMI correspond to trials of 2 classes (left-hand and right-hand imagery) collected from the EEG recordings of 54 participants, with 62 electrodes at a sampling frequency of 1000Hz. Each participant has data from two sessions and each session has two runs. The first run of each session is done in an offline manner, i.e. without feedback. The second run is done in an online manner, providing real-time visual feedback to the user. When not otherwise stated, we use a subset of 20 electrodes and we use the data from the two offline runs (i.e. the first run of the first and second session) for each participant, following the default settings of the MOABB [22] benchmark.

Preprocessing: Our preprocessing steps are the following: (i) we remove the 50Hz component through notch filtering (ii) we perform bandpass filtering (4Hz-38Hz) (iii) we resample the signals to 100Hz and (iv) for each trial, we crop a temporal window of 4 seconds, starting from its onset event. Upon obtaining the cropped trials, we use the session-wise covariance matrices of the EEG signals and perform Riemannian Alignment on the time-series of each trial, as in [57].

B. Comparison with other works and baseline

We compare our proposed method with four state-of-the-art techniques that provide their source code, namely Adaptive Transfer Learning (ATL) [54], EEGSym [38], TIDNet [28] and MIN2Net [4]. In order to fairly judge the impact of our proposed methodology, we also implement two additional methods: a single model baseline and an ensembling technique using the EEGNet architecture. The baseline method (mentioned as “EEGNet-Single”) is a single EEGNet model, that serves as a reference for the performance of an EEGNet architecture without ensembling. We implement the ensembling technique by training multiple individual EEGNet models. During inference, we fuse their predictions through a simple averaging operation, to obtain the final prediction. In essence, this method (mentioned as “EEGNet-Ensemble”) represents a post-training model ensemble. In the supplementary material, we provide more details about the implementations of all the aforementioned methods.

C. Evaluation settings

We perform evaluation in two ways: (i) in a 5-fold cross-validation (CV) manner and (ii) in a Leave-One-Subject-Out (LOSO) manner. In the 5-fold CV scenario, we split the subjects of our dataset into 5 disjoint folds and run 5 experiments. In each experiment, we use a different fold as our test set and then assign 3 folds to our training set and the 1 remaining fold to our validation set. In the LOSO scenario for a dataset with N subjects, we run N experiments where in the n -th experiment we use the data of the n -th subject as our test set. In each experiment, we split the remaining $N - 1$ subjects into our training and validation set. Specifically, we assign 80% of these subjects to the training set and the rest 20% to the validation set of the experiment. In both CV and LOSO scenarios, the reported accuracy is the average of the test accuracies across all experiments.

D. Training details

We train all models (i.e. our proposed method, the single model baseline and the model ensembling method) for 120 epochs with a batch size of 64. We use a Stochastic Gradient Descent (SGD) optimizer, setting the momentum to 0.9 and weight decay to 0.01. We initialize the learning rate at 0.01 for the first 60 epochs and then decrease it to 0.002 for the remaining 60 epochs.

E. Results (5-fold cross-validation)

In the first part of our experimental analysis we evaluate against methods that provide source code, under a 5-fold cross-validation scenario, without any model adaptation on test data or pretraining on external datasets. We note that these experiments are performed using exactly the same train, validation and test splits, the same trial length and the same number of electrodes for all methods (except for the method of EEGSym [38] that has an architectural requirement of 16 electrodes). Having the same experimental settings enables us to fairly judge the performance of all methods.

Table I shows the results of the methods trained on Physionet dataset with 5-fold cross-validation. Concerning our baseline method, we observe that a single EEGNet model achieves an accuracy of 82.09%. The standard model ensembling technique of EEGNet-Ensemble reaches an accuracy of 84.56% when fusing eight individual EEGNet models. Our proposed method presents a substantial boost of +1.80% over the standard ensemble scenario, reaching an accuracy of 86.36% when we use seven models at the first stage of our architecture. The model of EEGSym [38] achieves an accuracy of 83.91%, using $\sim 10\times$ more trainable parameters than the best performing architecture of our proposed method. EEGSym without pretraining on external data, performs worse than both our method and the standard model ensemble. Regarding the method of TIDNet [28], the accuracy of 82.19% is similar to that of our EEGNet-Single baseline model.

Table II shows the results of our 5-fold cross-validation experiment on OpenBMI for various methods. The baseline model of EEGNet-Single achieves an accuracy of 78.31% and the method of EEGNet-Ensemble provides a small boost of +0.67% when using eight individual EEGNet models, leading to an accuracy of 78.98%. Our proposed method performs superiorly, yielding an accuracy of 79.73% when using three first stage networks. The method of MIN2Net [4] has a low performance, with an accuracy of 69.44%. Regarding the method of ATL [54], the accuracy of 77.52% falls behind the results of both our proposed method and our baseline, using $\sim 60\times$ more trainable parameters than our proposed method. Our results show that a simple ensemble architecture trained with a curriculum learning scheme and an auxiliary loss can achieve high cross-subject generalization, without any adaptation on test data or complex model architecture.

Regarding the reported results of our proposed method in Table I and Table II, we note that the optimal number of first stage feature extractors K is inferred from the accuracy on the validation set. We provide more details about the impact of K on the performance of our architecture in Subsection IV-G

TABLE I: Performance of various methods on Physionet dataset, under 5-fold CV evaluation settings. The best accuracy is highlighted with bold.

| Method | Parameters | Accuracy (%) |
|---------------------------|------------|--------------|
| EEGNet-Single | 2.5K | 82.09 |
| EEGNet-Ensemble, 8 models | 20.0K | 84.56 |
| EEGSym [38] | 147.8K | 83.91 |
| TIDNet [28] | 694.2K | 82.19 |
| Ours, K=7 | 15.7K | 86.36 |

TABLE II: Performance of various methods on OpenBMI dataset, under 5-fold CV evaluation settings. The best accuracy is highlighted with bold.

| Method | Parameters | Accuracy (%) |
|---------------------------|------------|--------------|
| EEGNet-Single | 1.8K | 78.31 |
| EEGNet-Ensemble, 8 models | 14.3K | 78.98 |
| MIN2Net [4] | 37.1K | 69.44 |
| ATL [54] | 278.8K | 77.52 |
| Ours, K=3 | 4.6K | 79.73 |

(Table V and Table VI). Similarly, regarding the reported results of the EEGNet-Ensemble method in Table I and Table II, the optimal number of individual EEGNet models within an ensemble is chosen based on the validation accuracy. We elaborate on the results of the EEGNet-Ensemble method in the supplementary material.

F. Results (LOSO)

In this experiment, we compare our method against other state-of-the-art works that report LOSO results on Physionet and OpenBMI. We note that we mention the results of these methods as reported in their original works, ensuring that they do not utilise labelled data from the test subjects.

The results on Physionet dataset are shown in Table III. The method of EEGSym achieves state-of-the-art performance reaching an accuracy of 88.56%. EEGSym performs transfer learning by pretraining on four external datasets, which proves to be highly valuable. Our proposed method is the best performing model among the works that do not train on external data. We outperform the method of [7] that trains separate convolutional layers for each training subject. This further validates the existence of more efficient and accurate alternatives to complex deep architectures and the incorporation of subject-specific components.

The results on OpenBMI dataset are shown in Table IV. Our method presents state-of-the-art performance, scoring an accuracy of 85.07% when using all 62 electrodes of OpenBMI and having $K = 4$ first stage models. We outperform all other techniques, including the method of EEGSym that employs pretraining on external data. The geometric deep learning technique of TSMNet [26] and the algorithm of [30] that trains a convolutional architecture on spectral-spatial inputs, present an accuracy gap of more than $\sim 10\%$ from the methods of ATL, EEGSym and our technique. This indicates that deep architectures operating on covariance matrices of EEG time-series (e.g. [26] and [30]), are generally less suitable for cross-subject MI decoding, compared to architectures that operate on raw EEG time-series.

TABLE III: Comparison with other state-of-the-art methods on Physionet dataset with LOSO evaluation settings. The best accuracy is highlighted with bold.

*: pretrained on external data

| Method | Parameters | Accuracy (%) |
|----------------------------------|------------|--------------|
| OPS [49] - Human Neurosc. 2020 | N/A | 67.00 |
| Causal Viewpoint [7] - ICLR 2022 | N/A | 83.90 |
| EEGSym* [38] - TNSRE 2022 | 147K | 88.56 |
| Ours, K=7 | 15.7K | 85.82 |

TABLE IV: Comparison with other state-of-the-art methods on OpenBMI dataset with LOSO evaluation settings. The best accuracy is highlighted with bold.

*: pretrained on external data

| Method | Parameters | Accuracy (%) |
|------------------------------------|------------|--------------|
| MIN2Net [4] - TBME 2022 | 37.1K | 72.03 |
| Mutual Inf. [23] - TNNLS 2021 | N/A | 73.32 |
| Spectral-Spatial [30] - TNNLS 2019 | 77M | 74.15 |
| TSMNet [26] - NeurIPS 2022 | 4.5K | 74.60 |
| ATL [54] - Neural Networks 2021 | 305K | 84.19 |
| EEGSym* [38] - TNSRE 2022 | 147K | 84.72 |
| Ours, K=4 | 8.7K | 85.07 |

G. Ablation studies

In our ablation studies we investigate the impact of three components on the performance of our ensemble architecture. The first component is the number of first stage models K in the architecture. The second component is the loss $\mathcal{L}_{\text{subj}}^{\text{total}}$, that materializes our curriculum learning scheme. The third component is the distillation loss $\mathcal{L}_{\text{distill}}^{\text{total}}$ that enables collaborative training. We concurrently explore the effects of all these component choices, performing a sweep over the hyperparameter K and trying combinations of our loss terms.

Our first set of experiments (denoted as “ \mathcal{L}_{CE} ”) corresponds to the scenario of training a model ensemble architecture (as described in Sec. III-A2), i.e. without curriculum learning and without our distillation loss. In our second set of experiments (denoted as “ $\mathcal{L}_{\text{subj}}$ ”) we train our architecture with ensemble curriculum learning, as described in Sec. III-B, i.e. without our distillation loss. In the third experimental run (denoted as “ $\mathcal{L}_{\text{total}}$ ”) we apply our entire method (i.e. using both subject-weighted loss and intra-ensemble distillation loss), training our architecture with the loss of Eq. 14. All experiments are performed with a 5-fold cross-validation setting.

The results of our ablation study on Physionet dataset are shown in Table V. We observe a general trend of increasing accuracy for all our experimental sets, as K increases up to the value of 7 (further increasing K does not yield performance improvements). The only exception is the case where we train our architecture without curriculum learning (i.e. first row in Table V), where the accuracy saturates at $K = 6$. This indicates that training multiple feature extractors by equally fitting them to the entire training set, is a suboptimal approach of training on multiple source domains. Thus, applying our curriculum learning scheme through $\mathcal{L}_{\text{subj}}$ to induce diversity in the feature extractors, is a straightforward step. The results of the second row in Table V verify the positive impact of curriculum learning in our ensemble architecture. In some cases (i.e. when $K = 3$, $K = 4$ and $K = 6$) curriculum learning

TABLE V: Ablation study on Physionet dataset with 5-fold CV evaluation settings. Rows correspond to experiment sets done with different optimization objectives. Columns correspond to the number of first stage models (K) in our architecture. The best accuracy of each row is highlighted with bold.

| Loss terms | Accuracy (%) | | | | | |
|-----------------------|--------------|-------|-------|-------|--------------|--------------|
| | K=2 | K=3 | K=4 | K=5 | K=6 | K=7 |
| \mathcal{L}_{CE} | 83.34 | 84.70 | 84.97 | 84.93 | 85.53 | 85.34 |
| \mathcal{L}_{subj} | 84.38 | 84.72 | 85.10 | 85.40 | 85.62 | 85.68 |
| \mathcal{L}_{total} | 83.76 | 84.78 | 85.02 | 85.48 | 86.04 | 86.36 |

TABLE VI: Ablation study on OpenBMI dataset with 5-fold CV evaluation settings. Rows correspond to experiment sets done with different optimization objectives. Columns correspond to the number of first stage models (K) in our architecture. The best accuracy of each row is highlighted with bold.

| Loss terms | Accuracy (%) | | | | | |
|-----------------------|--------------|--------------|-------|--------------|-------|-------|
| | K=2 | K=3 | K=4 | K=5 | K=6 | K=7 |
| \mathcal{L}_{CE} | 79.15 | 79.08 | 78.96 | 79.24 | 78.94 | 79.20 |
| \mathcal{L}_{subj} | 79.02 | 79.58 | 79.13 | 79.15 | 79.01 | 79.31 |
| \mathcal{L}_{total} | 79.25 | 79.73 | 79.53 | 79.46 | 79.10 | 79.66 |

provides negligible accuracy gains. When further incorporating our distillation loss in the total optimization objective of our architecture (i.e. third row in Table V), we get additional accuracy boosts, except for the cases of $K = 2$ and $K = 4$. The beneficial effect of regulating the balance between feature diversity and model generalization through our distillation loss, is higher in the cases of $K = 6$ and $K = 7$ where the accuracy boosts are +0.42% and +0.68% respectively. This finding is particularly interesting, showing that the combination of our two loss terms can increase the performance of model ensembles, even when using many feature extraction models. On the contrary, an ensemble architecture trained solely with the standard cross-entropy loss, is more prone to performance saturation.

The results of our ablation study on OpenBMI dataset are shown in Table VI. The standard ensemble architecture trained without curriculum learning (i.e. first row in Table VI) achieves a maximum accuracy of 79.24% when $K = 5$. By using our curriculum learning scheme, we improve the accuracy of our architecture in four out of six cases, achieving a maximum accuracy of 79.58% when $K = 3$. The incorporation of our distillation loss term in the total loss of our architecture (i.e. third row in Table VI) provides consistent improvements in all cases. Our best model has an accuracy of 79.73% when $K = 3$, with a boost of 0.65% over its corresponding standard ensemble model.

V. CONCLUSION

In this work, we propose a method for cross-subject motor imagery decoding that leverages the combined strengths of model ensembling, curriculum learning and collaborative training. We design an ensemble architecture that is trained end-to-end in a single phase. We show that our curriculum training scheme can induce diversity to the feature extraction models of our architecture, improving its performance over standard

ensembling. Our method also benefits from the exchange of knowledge between the models of our ensemble, that occurs through our auxiliary distillation loss. We conduct experiments on the datasets of Physionet [16] and OpenBMI [32], totalling more than 150 participants, and demonstrate state-of-the-art results. Our proposed method outperforms other approaches that try to tackle MI decoding using complex networks [28], [54], multi-task learning [4], geometric deep learning [26], subject-specific layers [7] or pretraining on multiple external datasets [38]. Our work highlights the importance of feature diversity as a property of model ensembles, paving the way for robust EEG-based domain generalization techniques.

REFERENCES

- [1] R. Abiri, S. Borhani, E. W. Sellers, Y. Jiang, and X. Zhao. A comprehensive review of eeg-based brain-computer interface paradigms. *Journal of neural engineering*, 16(1):011001, 2019.
- [2] G. A. Altuwaijri, G. Muhammad, H. Altaheri, and M. Alsulaiman. A multi-branch convolutional neural network with squeeze-and-excitation attention blocks for eeg-based motor imagery signals classification. *Diagnostics*, 12(4):995, 2022.
- [3] K. K. Ang, Z. Y. Chin, H. Zhang, and C. Guan. Filter bank common spatial pattern (fbcsp) in brain-computer interface. In *2008 IEEE international joint conference on neural networks (IEEE world congress on computational intelligence)*, pages 2390–2397. IEEE, 2008.
- [4] P. Autthasan, R. Chaisaen, T. Sudhawiyangkul, P. Rangpong, S. Kitthaveephong, N. Dilokthanakul, G. Bhakdisongkhram, H. Phan, C. Guan, and T. Wilaiprasitporn. Min2net: End-to-end multi-task learning for subject-independent motor imagery eeg classification. *IEEE Transactions on Biomedical Engineering*, 69(6):2105–2118, 2021.
- [5] S. Bakas, S. Ludwig, K. Barnmpas, M. Bahri, Y. Panagakis, N. Laskaris, D. A. Adamos, and S. Zafeiriou. Team cogitat at neurips 2021: Benchmarks for eeg transfer learning competition. *arXiv preprint arXiv:2202.03267*, 2022.
- [6] P. D. E. Baniqued, E. C. Stanyer, M. Awais, A. Alazmani, A. E. Jackson, M. A. Mon-Williams, F. Mushtaq, and R. J. Holt. Brain-computer interface robotics for hand rehabilitation after stroke: A systematic review. *Journal of NeuroEngineering and Rehabilitation*, 18(1):1–25, 2021.
- [7] K. Barnmpas, Y. Panagakis, D. Adamos, N. Laskaris, and S. Zafeiriou. A causal viewpoint on motor-imagery brainwave decoding. In *ICLR2022 Workshop on the Elements of Reasoning: Objects, Structure and Causality*, 2022.
- [8] H. Berger. Über das elektroenkephalogramm des menschen. *Archiv für psychiatrie und nervenkrankheiten*, 87(1):527–570, 1929.
- [9] Y. Bian and H. Chen. When does diversity help generalization in classification ensembles? *IEEE Transactions on Cybernetics*, 2021.
- [10] B. Blankertz, R. Tomioka, S. Lemm, M. Kawanabe, and K.-R. Müller. Optimizing spatial filters for robust eeg single-trial analysis. *IEEE Signal processing magazine*, 25(1):41–56, 2007.
- [11] L. Breiman. Bagging predictors. *Machine learning*, 24(2):123–140, 1996.
- [12] D. D. Chakladar, S. Dey, P. P. Roy, and M. Iwamura. Eeg-based cognitive state assessment using deep ensemble model and filter bank common spatial pattern. In *2020 25th International Conference on Pattern Recognition (ICPR)*, pages 4107–4114. IEEE, 2021.
- [13] X. Chen and K. He. Exploring simple siamese representation learning. In *Proceedings of the IEEE/CVF Conference on Computer Vision and Pattern Recognition*, pages 15750–15758, 2021.
- [14] I. Dolzhikova, B. Abibullaev, R. Sameni, and A. Zollanvari. An ensemble cnn for subject-independent classification of motor imagery-based eeg. In *2021 43rd Annual International Conference of the IEEE Engineering in Medicine & Biology Society (EMBC)*, pages 319–324. IEEE, 2021.
- [15] Y. Du and J. Liu. Ienet: a robust convolutional neural network for eeg based brain-computer interfaces. *Journal of Neural Engineering*, 2022.
- [16] A. L. Goldberger, L. A. Amaral, L. Glass, J. M. Hausdorff, P. C. Ivanov, R. G. Mark, J. E. Mietus, G. B. Moody, C.-K. Peng, and H. E. Stanley. Physiobank, physiotoolkit, and physionet: components of a new research resource for complex physiologic signals. *circulation*, 101(23):e215–e220, 2000.
- [17] I. Gulrajani and D. Lopez-Paz. In search of lost domain generalization. In *9th International Conference on Learning Representations, ICLR 2021, Virtual Event, Austria, May 3-7, 2021*. OpenReview.net, 2021.

- [18] L. K. Hansen and P. Salamon. Neural network ensembles. *IEEE transactions on pattern analysis and machine intelligence*, 12(10):993–1001, 1990.
- [19] H. He and D. Wu. Transfer learning for brain–computer interfaces: A euclidean space data alignment approach. *IEEE Transactions on Biomedical Engineering*, 67(2):399–410, 2019.
- [20] F. A. Heilmeyer, R. T. Schirrmeyer, L. D. Fiederer, M. Volker, J. Behncke, and T. Ball. A large-scale evaluation framework for eeg deep learning architectures. In *2018 IEEE International Conference on Systems, Man, and Cybernetics (SMC)*, pages 1039–1045. IEEE, 2018.
- [21] É. R. M. Heremans, H. Phan, P. Borzée, B. Buysse, D. Testelmans, and M. De Vos. From unsupervised to semi-supervised adversarial domain adaptation in eeg-based sleep staging. *Journal of Neural Engineering*, 2022.
- [22] V. Jayaram and A. Barachant. Moabb: trustworthy algorithm benchmarking for bcis. *Journal of neural engineering*, 15(6):066011, 2018.
- [23] E. Jeon, W. Ko, J. S. Yoon, and H.-I. Suk. Mutual information-driven subject-invariant and class-relevant deep representation learning in bci. *IEEE Transactions on Neural Networks and Learning Systems*, 2021.
- [24] C. Jeunet, F. Lotte, M. Hachet, and B. N’Kaoua. Impact of cognitive and personality profiles on motor-imagery based brain-computer interface-controlling performance. In *17th World Congress of Psychophysiology (IOP2014)*, 2014.
- [25] C. Jeunet, B. N’Kaoua, S. Subramanian, M. Hachet, and F. Lotte. Predicting mental imagery-based bci performance from personality, cognitive profile and neurophysiological patterns. *PLoS one*, 10(12):e0143962, 2015.
- [26] R. J. Kobler, J.-i. Hirayama, Q. Zhao, and M. Kawanabe. Spd domain-specific batch normalization to crack interpretable unsupervised domain adaptation in eeg. *arXiv preprint arXiv:2206.01323*, 2022.
- [27] Z. J. Koles. The quantitative extraction and topographic mapping of the abnormal components in the clinical eeg. *Electroencephalography and clinical Neurophysiology*, 79(6):440–447, 1991.
- [28] D. Kostas and F. Rudzicz. Thinker invariance: enabling deep neural networks for bci across more people. *Journal of Neural Engineering*, 17(5):056008, 2020.
- [29] L. Kuhlmann, P. Karoly, D. R. Freestone, B. H. Brinkmann, A. Temko, A. Barachant, F. Li, G. Titericz Jr, B. W. Lang, D. Lavery, et al. Epilepsycosystem.org: crowd-sourcing reproducible seizure prediction with long-term human intracranial eeg. *Brain*, 141(9):2619–2630, 2018.
- [30] O.-Y. Kwon, M.-H. Lee, C. Guan, and S.-W. Lee. Subject-independent brain–computer interfaces based on deep convolutional neural networks. *IEEE transactions on neural networks and learning systems*, 31(10):3839–3852, 2019.
- [31] V. J. Lawhern, A. J. Solon, N. R. Waytowich, S. M. Gordon, C. P. Hung, and B. J. Lance. Eegnet: a compact convolutional neural network for eeg-based brain–computer interfaces. *Journal of neural engineering*, 15(5):056013, 2018.
- [32] M.-H. Lee, O.-Y. Kwon, Y.-J. Kim, H.-K. Kim, Y.-E. Lee, J. Williamson, S. Fazli, and S.-W. Lee. Eeg dataset and openbmi toolbox for three bci paradigms: An investigation into bci illiteracy. *GigaScience*, 8(5):giz002, 2019.
- [33] J. Li, S. Qiu, C. Du, Y. Wang, and H. He. Domain adaptation for eeg emotion recognition based on latent representation similarity. *IEEE Transactions on Cognitive and Developmental Systems*, 12(2):344–353, 2019.
- [34] M. Lotze and L. G. Cohen. Volition and imagery in neurorehabilitation. *Cognitive and behavioral neurology*, 19(3):135–140, 2006.
- [35] B.-Q. Ma, H. Li, W.-L. Zheng, and B.-L. Lu. Reducing the subject variability of eeg signals with adversarial domain generalization. In *International Conference on Neural Information Processing*, pages 30–42. Springer, 2019.
- [36] W. Ma, H. Xue, X. Sun, S. Mao, L. Wang, Y. Liu, Y. Wang, and X. Lin. A novel multi-branch hybrid neural network for motor imagery eeg signal classification. *Biomedical Signal Processing and Control*, 77:103718, 2022.
- [37] S.-H. Park, D. Lee, and S.-G. Lee. Filter bank regularized common spatial pattern ensemble for small sample motor imagery classification. *IEEE Transactions on Neural Systems and Rehabilitation Engineering*, 26(2):498–505, 2017.
- [38] S. Pérez-Velasco, E. Santamaría-Vázquez, V. Martínez-Cagigal, D. Marcos-Martínez, and R. Hornero. Eegsym: Overcoming inter-subject variability in motor imagery based bcis with deep learning. *IEEE Transactions on Neural Systems and Rehabilitation Engineering*, 30:1766–1775, 2022.
- [39] C. Reuben, P. Karoly, D. R. Freestone, A. Temko, A. Barachant, F. Li, G. Titericz Jr, B. W. Lang, D. Lavery, K. Roman, et al. Ensembling crowdsourced seizure prediction algorithms using long-term human intracranial eeg. *Epilepsia*, 61(2):e7–e12, 2020.
- [40] S. Rimbart, D. Trocellier, and F. Lotte. Is event-related desynchronization variability correlated with bci performance? In *2022 IEEE International Conference on Metrology for eXtended Reality, Artificial Intelligence, and Neural Engineering*, 2022.
- [41] C. Sannelli, C. Vidaurre, K.-R. Müller, and B. Blankertz. Csp patches: an ensemble of optimized spatial filters. an evaluation study. *Journal of Neural Engineering*, 8(2):025012, 2011.
- [42] G. Schalk, D. J. McFarland, T. Hinterberger, N. Birbaumer, and J. R. Wolpaw. Bci2000: a general-purpose brain-computer interface (bci) system. *IEEE Transactions on biomedical engineering*, 51(6):1034–1043, 2004.
- [43] R. T. Schirrmeyer, J. T. Springenberg, L. D. J. Fiederer, M. Glasstetter, K. Eggensperger, M. Tangermann, F. Hutter, W. Burgard, and T. Ball. Deep learning with convolutional neural networks for eeg decoding and visualization. *Human brain mapping*, 38(11):5391–5420, 2017.
- [44] A. Soria-Frisch. A critical review on the usage of ensembles for bci. *Towards Practical Brain-Computer Interfaces*, pages 41–65, 2012.
- [45] M. Spape, K. Davis, L. Kangassalo, N. Ravaja, Z. Sovijarvi-Spape, and T. Ruotsalo. Brain-computer interface for generating personally attractive images. *IEEE Transactions on Affective Computing*, 1(1), 2021.
- [46] V. Vapnik. *Statistical learning theory*. Wiley, 1998.
- [47] J. Wang, C. Lan, C. Liu, Y. Ouyang, T. Qin, W. Lu, Y. Chen, W. Zeng, and P. Yu. Generalizing to unseen domains: A survey on domain generalization. *IEEE Transactions on Knowledge and Data Engineering*, 2022.
- [48] X. Wei, P. Ortega, and A. A. Faisal. Inter-subject deep transfer learning for motor imagery eeg decoding. In *2021 10th International IEEE/EMBS Conference on Neural Engineering (NER)*, pages 21–24. IEEE, 2021.
- [49] L. Xu, M. Xu, Y. Ke, X. An, S. Liu, and D. Ming. Cross-dataset variability problem in eeg decoding with deep learning. *Frontiers in human neuroscience*, 14:103, 2020.
- [50] M. Xu, J. Han, Y. Wang, T.-P. Jung, and D. Ming. Implementing over 100 command codes for a high-speed hybrid brain-computer interface using concurrent p300 and ssvep features. *IEEE Transactions on Biomedical Engineering*, 67(11):3073–3082, 2020.
- [51] D. Yadav, S. Yadav, and K. Veer. A comprehensive assessment of brain computer interfaces: Recent trends and challenges. *Journal of Neuroscience Methods*, 346:108918, 2020.
- [52] H. Yuan and B. He. Brain–computer interfaces using sensorimotor rhythms: current state and future perspectives. *IEEE Transactions on Biomedical Engineering*, 61(5):1425–1435, 2014.
- [53] H. Zhang, M. Cissé, Y. N. Dauphin, and D. Lopez-Paz. mixup: Beyond empirical risk minimization. In *6th International Conference on Learning Representations, ICLR 2018, Vancouver, BC, Canada, April 30 - May 3, 2018, Conference Track Proceedings*, 2018.
- [54] K. Zhang, N. Robinson, S.-W. Lee, and C. Guan. Adaptive transfer learning for eeg motor imagery classification with deep convolutional neural network. *Neural Networks*, 136:1–10, 2021.
- [55] K. Zhou, Y. Yang, Y. Qiao, and T. Xiang. Domain adaptive ensemble learning. *IEEE Transactions on Image Processing*, 30:8008–8018, 2021.
- [56] H. Zhu, D. Forenzo, and B. He. On the deep learning models for eeg-based brain-computer interface using motor imagery. *IEEE Transactions on Neural Systems and Rehabilitation Engineering*, 2022.
- [57] G. Zoumpourlis and I. Patras. Covmix: Covariance mixing regularization for motor imagery decoding. In *2022 10th International Winter Conference on Brain-Computer Interface (BCI)*, pages 1–7. IEEE, 2022.

VI. SUPPLEMENTARY MATERIAL

In the supplementary material, we first provide details about our proposed curriculum learning scheme in Section VI-A. Then, in the following sections we describe the architecture and training process of various methods, namely: i) a baseline method of a single EEGNet [31] model (Section VI-B), ii) two model ensembling methods (Section VI-C) and iii) our proposed model ensemble architecture (Section VI-D). Moreover, in Section VI-E we present experimental results of the two model ensembling methods. These results can serve as additional references against which the results of our proposed method can be compared. Finally, in Section VI-F we provide details on the training process that we follow in order to reproduce four state-of-the-art techniques for motor imagery decoding, namely Adaptive Transfer Learning (ATL) [54], EEGSym [38], TIDNet [28] and MIN2Net [4].

A. Ensemble curriculum learning

In Fig. 2 of our main paper we present the training pipeline of our architecture that employs an ensemble curriculum learning scheme and a distillation loss. We also describe the subject-weighted loss that materializes our curriculum learning scheme in Subsection III-B of our main paper and present its formula in Eq. 9 of our main paper. To allow a better understanding of the coefficient $\beta(\mathbf{x}, k)$ that is involved in Eq. 9 of our main paper, we show an overview of our curriculum learning scheme in Fig. 3. Specifically, we consider an example where we are provided with a dataset \mathcal{D} containing EEG data from 10 human subjects and our proposed model ensemble architecture consists of $K = 3$ models. The dataset $\mathcal{D} = \{\mathcal{D}_1, \mathcal{D}_2, \dots, \mathcal{D}_{10}\}$ containing the sub-datasets of 10 subjects is split into $K = 3$ non-overlapping subsets: \mathcal{S}_1 , \mathcal{S}_2 and \mathcal{S}_3 . Our curriculum learning scheme aims to make the k -th model to specialize on the subjects belonging to subset \mathcal{S}_k of \mathcal{D} , while still training on the whole dataset \mathcal{D} . This is done using the coefficient $\beta(\mathbf{x}, k)$ that controls the loss contribution of a training sample \mathbf{x} on the weight updating process for the k -th model. To achieve specialization on the samples of \mathcal{S}_k , when $\mathbf{x} \in \mathcal{S}_k$, we set $\beta(\mathbf{x}, k) = 1$ throughout the training process. We also want to train the k -th model on the rest of the subjects of \mathcal{D} (i.e. those that do not belong to \mathcal{S}_k), albeit with a progressively decreasing loss contribution over time. For this reason, when $\mathbf{x} \notin \mathcal{S}_k$ we set $\beta(\mathbf{x}, k) = \alpha$, with α decaying from 1 to 0 while training progresses.

B. Single model baseline

EEGNet-Single: Our baseline method (mentioned as “EEGNet-Single”) is a single EEGNet model, trained in the entire training set as described in Subsection III-A1 of our main paper. The detailed architecture of EEGNet is shown in Table VII.

C. Model ensembling methods

EEGNet-Ensemble: We implement the first ensembling method by training multiple individual EEGNet models in the entire training set. During inference, we fuse their predictions

through a simple averaging operation to obtain the final prediction. In essence, this ensembling method (mentioned as “EEGNet-Ensemble”) represents a post-training model ensemble.

EEGNet-Bagging: We implement the second ensembling method by training multiple individual EEGNet models in random subsets of the training set. Specifically, we train each individual EEGNet model on 85% of all the available training subjects. We choose the subjects to be kept for training in each experiment, by simply performing random subsampling. During inference, we fuse the predictions of all models through an averaging operation to obtain the final prediction. This method (mentioned as “EEGNet-Bagging”) represents the well-known ensembling technique of bootstrap aggregating [11]. We note that we report results using this ensembling method in this supplementary material, for the sake of a more complete evaluation, albeit not including this method in the main manuscript of our work.

D. Proposed model

Our proposed model ensemble architecture, described in Subsection III-A2 of our main paper, consists of two stages and uses EEGNet as its elementary component. The first stage of our proposed architecture contains multiple feature extractors in parallel, with each first stage network producing a feature vector. Considering the EEGNet architecture that is presented in Table VII, each first stage network of our architecture contains all the layers up to (and including) the feature flattening layer of EEGNet. The second stage has a single shared classification head that computes the class-wise prediction scores for each feature vector originating from the first stage. Based on the EEGNet layers that are presented in Table VII, the second stage of our architecture corresponds to the last layer of EEGNet, i.e. a single fully connected layer that performs classification.

E. Experimental results (5-fold cross-validation)

In the first part of the experimental analysis presented in our main paper, we compare our proposed method against our single model baseline as well as the standard model ensembling method, under a 5-fold cross-validation scenario. We note that these experiments are performed using exactly the same train, validation and test splits. Here we provide additional results, presenting the performance of the EEGNet-Ensemble and EEGNet-Bagging methods as the number M of individual EEGNet models varies.

EEGNet-Ensemble: In Table VIII we show the cross-subject performance of EEGNet-Ensemble on Physionet dataset under a 5-fold cross-validation scenario, when using from 2 to 9 EEGNet models. The best accuracy (84.56%) is achieved when fusing the predictions from 8 EEGNet models. In Table IX we show the cross-subject performance of EEGNet-Ensemble on OpenBMI dataset under a 5-fold cross-validation scenario, when using from 2 to 9 EEGNet models. The best accuracy (78.98%) is achieved when fusing the predictions from 8 EEGNet models.

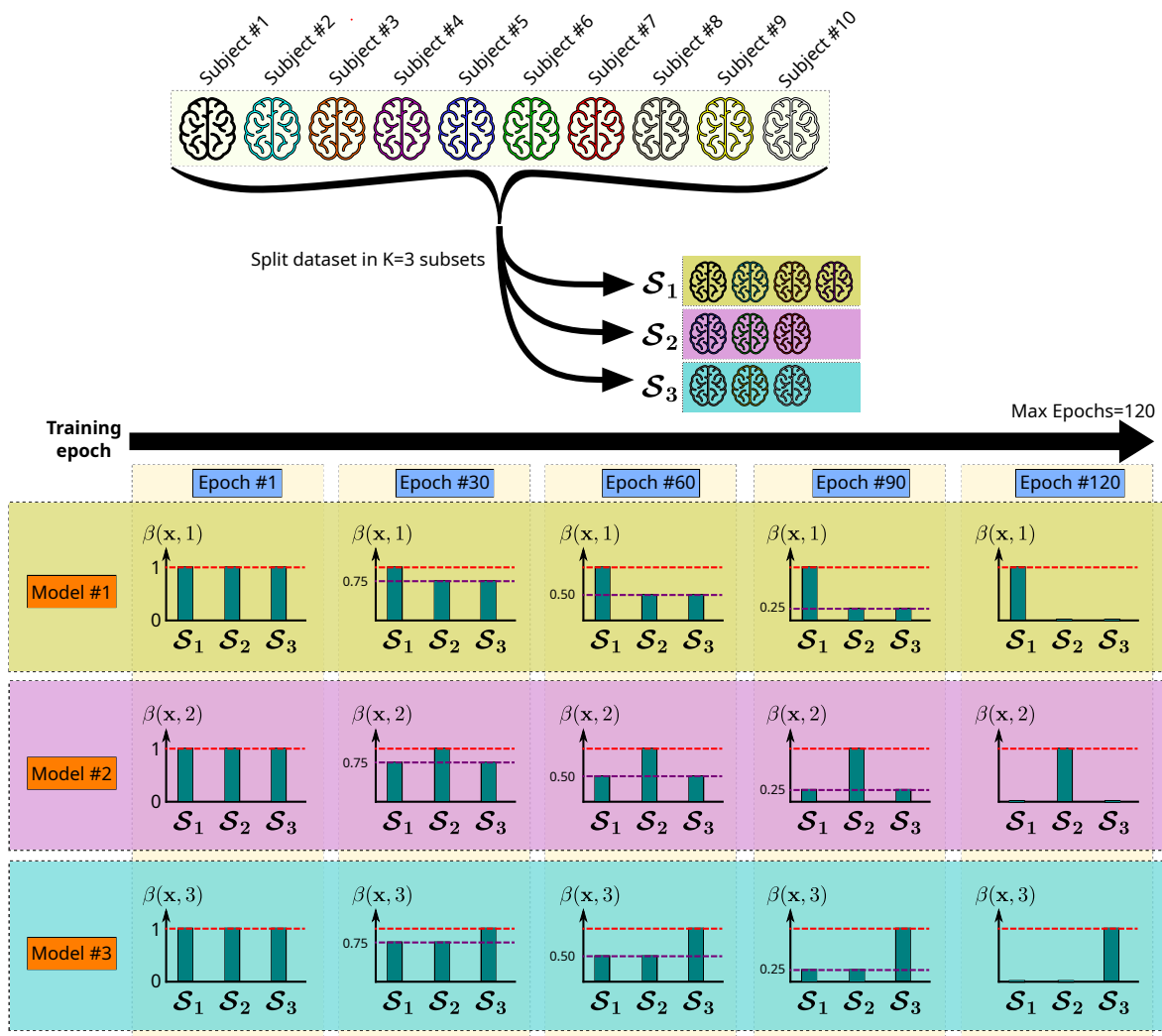


Fig. 3: Indicative illustration of our curriculum learning scheme. In this example, we are provided with a dataset \mathcal{D} containing EEG data from 10 human subjects and our proposed model ensemble architecture consists of $K = 3$ models.

TABLE VII: Architecture of a single EEGNet model. The input of the model has a shape of $B \times 1 \times C \times T$, where B is the batch size, C is the number of EEG electrodes and T is the number of samples in the temporal dimension. The output of the model has a shape of $B \times 2$, in the case of two output classes.

| Layer | Input shape | Output shape |
|---|------------------------------------|------------------------------------|
| Dropout ($p=0.4$) | $B \times 1 \times C \times T$ | $B \times 1 \times C \times T$ |
| Temporal Convolution, 8 filters kernel=(1, 64), stride=(1, 1), pad=(0, 32) | $B \times 1 \times C \times T$ | $B \times 8 \times C \times T$ |
| Spatial Convolution, 16 filters kernel=(1, C), stride=(1, 1), pad=(0, 0) max. weight norm=1.0 | $B \times 8 \times C \times T$ | $B \times 16 \times 1 \times T$ |
| Temporal Pooling kernel=(1, 4), stride=(1, 4), pad=(0, 0) | $B \times 16 \times 1 \times T$ | $B \times 16 \times 1 \times T$ |
| Batch Normalization 2D | $B \times 16 \times 1 \times T/4$ | $B \times 16 \times 1 \times T/4$ |
| ELU activation | $B \times 16 \times 1 \times T/4$ | $B \times 16 \times 1 \times T/4$ |
| Dropout ($p=0.1$) | $B \times 16 \times 1 \times T/4$ | $B \times 16 \times 1 \times T/4$ |
| Separable Convolution Depthwise, 16 filters, 16 groups kernel=(1, 16), stride=(1, 1), pad=(0, 8) | $B \times 16 \times 1 \times T/4$ | $B \times 16 \times 1 \times T/4$ |
| Separable Convolution Pointwise, 16 filters, 16 groups kernel=(1, 1), stride=(1, 1), pad=(0, 0) | $B \times 16 \times 1 \times T/4$ | $B \times 16 \times 1 \times T/4$ |
| Batch Normalization 2D | $B \times 16 \times 1 \times T/4$ | $B \times 16 \times 1 \times T/4$ |
| ReLU activation | $B \times 16 \times 1 \times T/4$ | $B \times 16 \times 1 \times T/4$ |
| Temporal Pooling kernel=(1, 8), stride=(1, 8), pad=(0, 0) | $B \times 16 \times 1 \times T/4$ | $B \times 16 \times 1 \times T/32$ |
| Flatten | $B \times 16 \times 1 \times T/32$ | $B \times T/2$ |
| Fully Connected | $B \times T/2$ | $B \times 2$ |

EEGNet-Bagging: In Table X we show the cross-subject performance of EEGNet-Bagging on Physionet dataset under a 5-fold cross-validation scenario, when using from 2 to 9 EEGNet models. The best accuracy (84.81%) is achieved when using the predictions from 8 EEGNet models. In Table XI we show the cross-subject performance of EEGNet-Bagging on OpenBMI dataset under a 5-fold cross-validation scenario, when using from 2 to 9 EEGNet models. The best accuracy (79.28%) is achieved when using the predictions from 7 EEGNet models.

TABLE VIII: Performance of EEGNet-Ensemble on Physionet dataset with 5-fold cross-validation evaluation settings. Columns correspond to the number of individual EEGNet models (M) that we use. The best accuracy is highlighted with bold.

| Accuracy (%) | | | | | | | |
|--------------|-------|-------|-------|-------|-------|--------------|-------|
| M=2 | M=3 | M=4 | M=5 | M=6 | M=7 | M=8 | M=9 |
| 82.99 | 84.01 | 84.10 | 84.21 | 84.04 | 84.26 | 84.56 | 84.47 |

TABLE IX: Performance of EEGNet-Ensemble on OpenBMI dataset with 5-fold cross-validation evaluation settings. Columns correspond to the number of individual EEGNet models (M) that we use. The best accuracy is highlighted with bold.

| Accuracy (%) | | | | | | | |
|--------------|-------|-------|-------|-------|-------|--------------|-------|
| M=2 | M=3 | M=4 | M=5 | M=6 | M=7 | M=8 | M=9 |
| 78.95 | 78.91 | 78.86 | 78.93 | 78.91 | 78.95 | 78.98 | 78.97 |

TABLE X: Performance of EEGNet-Bagging on Physionet dataset with 5-fold cross-validation evaluation settings. Columns correspond to the number of individual EEGNet models (M) that we use. The best accuracy is highlighted with bold.

| Accuracy (%) | | | | | | | |
|--------------|-------|-------|-------|-------|-------|--------------|-------|
| M=2 | M=3 | M=4 | M=5 | M=6 | M=7 | M=8 | M=9 |
| 83.05 | 84.22 | 84.17 | 84.49 | 84.68 | 84.73 | 84.81 | 84.74 |

TABLE XI: Performance of EEGNet-Bagging on OpenBMI dataset with 5-fold cross-validation evaluation settings. Columns correspond to the number of individual EEGNet models (M) that we use. The best accuracy is highlighted with bold.

| Accuracy (%) | | | | | | | |
|--------------|-------|-------|-------|-------|--------------|-------|-------|
| M=2 | M=3 | M=4 | M=5 | M=6 | M=7 | M=8 | M=9 |
| 78.99 | 79.00 | 79.18 | 79.26 | 79.20 | 79.28 | 79.07 | 79.11 |

F. Training details of state-of-the-art methods

In our main paper, we compare our proposed method with four state-of-the-art techniques that provide their source code, namely Adaptive Transfer Learning (ATL) [54], EEGSym [38], TIDNet [28] and MIN2Net [4]. In the following paragraphs, we briefly refer to the details of the training settings for each technique, regarding our 5-fold cross-validation experiments. In general, we keep the same

hyperparameter choices with the original works, except from the temporal duration of the trials, which we set equal to 4.0 seconds for all methods for fair comparison.

ATL: We use the official implementation² of ATL [54]. The method employs the Deep4Net [43] model architecture, as defined in `braindecode`³ toolbox. We perform subject-independent training, i.e. no data from the test subjects are used during training. We train all models for 200 epochs with a batch size of 16. We use an AdamW optimizer, with a learning rate of 0.01 and a weight decay of 0.0005. We also use a temporal length of 4 seconds for all trials.

EEGSym: We use the official implementation⁴ of EEGSym [38]. The method employs the custom model architecture that is described in the original publication [38]. The model architecture does not support an arbitrary number of input EEG electrode channels, restricting the options to 8 or 16 electrodes. We choose to use 16 electrodes, to retain more information in the input EEG signals. To ensure fair comparison with other methods and our models, we do not use the model weights that are provided, as they are obtained by pretraining on four external datasets. We perform training for 500 epochs with a batch size of 32, and set the patience for early stopping to 25 epochs. We use Cross-Entropy as the loss function and employ an Adam optimizer with a learning rate of 0.001. We set the dropout rate to 0.4 and use 24 filters per branch in the model architecture. We also use a temporal length of 4 seconds for all trials.

TIDNet: We use the official implementation⁵ of TIDNet [28]. We train the TIDNet architecture for 30 epochs using a batch size of 16. We perform MixUp setting its hyperparameter β equal to 8.0, and employ Euclidean Alignment on the EEG time-series. We use a temporal length of 4 seconds for all trials. We use the Kullback–Leibler (KL) divergence as the loss function. In each epoch, we perform evaluation using the Exponentially Weighted Moving Average (EWMA) of the model weights from the last 5 epochs.

MIN2Net: We use the official implementation⁶ of MIN2Net [4]. We train the MIN2Net model architecture for 200 epochs with a batch size of 100. We set the initial learning rate to 0.001 and decay the learning rate by a factor of 0.5, with a patience of 20 epochs. The minimum learning rate is set equal to 0.0001. We set the hyperparameters of MIN2Net as follows: $\alpha = 1.0$, $\beta_1 = 0.5$, $\beta_2 = 0.5$ and $\beta_3 = 1.0$. We use a temporal length of 4 seconds for all trials.

²<https://github.com/zhangks98/eeg-adapt>

³<https://github.com/braindecode/braindecode>

⁴<https://github.com/Serpeve/EEGSym>

⁵<https://github.com/SPOClab-ca/ThinkerInvariance>

⁶<https://github.com/IoBT-VISTEC/MIN2Net>